Characteristics of 3000 bar Diesel Spray Injection under Non-Vaporizing and Vaporizing Conditions

Jaclyn E. Johnson[1], Seung Hyun Yoon[1], Jeffrey D. Naber[1], Seong-Young Lee[1], Gary Hunter[2], Russell Truemner[2], Tony Harcombe [3]*
[1]Michigan Technological University
Mechanical Engineering – Engineering Mechanics Department
Houghton, MI 49931, USA
[2]AVL Powertrain Engineering, Inc.
Plymouth, MI 48170, USA
[3]Delphi Diesel Systems
London W3 OSE, England

Abstract

Increasing fuel injection pressure has enabled continuous reduction of diesel emissions while sustaining the high thermal efficiency advantage of diesel engines. Current production diesel injectors operate in the range from 300 to 2000 bar. The ongoing trend for fuel injection systems is to higher injection pressures and smaller nozzle hole diameters for further emissions reduction and fuel efficiency improvements. Fundamental understanding of diesel spray characteristics including liquid penetration and cone angle is imperative to improve model development and facilitate the integration of elevated injection pressure systems into future diesel engines.

Studies were conducted in an optically accessible constant volume combustion vessel under non-vaporizing and vaporizing conditions. A 7-hole injector, currently being developed for high injection pressure applications, was studied between 2000 and 3000 bar injection pressures with ultra-low sulfur diesel fuel. The study included two part-load charge density conditions of 7.4 kg/m^3 and 14.7 kg/m^3 along with an elevated density boosted condition of 34.8 kg/m^3. Diagnostics used included Mie back scatter imaging for liquid phase penetration. Experimental results were compared to spray penetration relationships to extrapolate these relationships to the elevated injection pressure conditions. Thus, an improved understanding of the influence of elevated injection pressure on fundamental spray characteristics was gained.

Introduction

Diesel combustion and emissions are spray and mixing controlled where the influence of operating parameters, i.e. injection pressure and ambient density, on spray characteristics are significant. One approach to further improve the efficiency of diesel engines is to increase injection pressures with the premise of promoting fuel air mixing [1]. Diesel injection system maximum pressure capabilities have increased from 800 to 2000 bar over the last 10 years, and more recently, higher injection pressures up to 2400 bar have been realized with advanced common rail-systems and smaller nozzles. Injection pressures are likely to increase to 3000 bar by 2015 and 4000 bar by 2020 [2]. Through increases in injection pressure in conjunction with optimized nozzle geometries, designs and other engine advancements, an additional 4% improvement in fuel efficiency may be realized [3]. In addition to the fuel efficiency improvement, exhaust emission standards may be met, with less after-treatment needed by increasing injection pressures up to 3000 bar levels while simultaneously improving and enhancing nozzle geometry [4]. Based on these trends, an injector was studied in an effort to understand the influence of elevated injection pressures, up to 3000 bar, on spray characteristics under typical engine conditions. Experimental results obtained from Mie back scatter imaging in an optically accessible combustion vessel were quantified and analyzed. In addition, the results were compared to correlations used for predicting penetration and liquid length, to understand their application to elevated injection pressures of 2000 bar and above.

Experimental Setup

Experimental tests were conducted in the optically accessible constant volume chamber shown in Figure 1. The vessel has an internal volume of approximately 1 liter, six face-ports housing three sapphire windows, a spark plug – dual fan port, a diesel fuel injector port (Figure 1), and one blank port. Additionally, there are eight access ports on the combustion vessel (CV) cube vertices containing a pressure transducer, inlet and exhaust valves, and blanks. Tests are conducted in an inert environment achieved by filling the combustion vessel with

* Corresponding Author: jenesbit@mtu.edu

nitrogen (CV electrically heated to 373 K) or in a zero percent oxygen vaporizing environment (CV electrically heated to 453 K), achieved through the use of a preburn procedure [5-7]. This procedure produces representative diesel engine conditions in the combustion chamber including pressure, temperature, and density. The process involves spark igniting a fuel-lean acetylene, hydrogen, oxygen and nitrogen gaseous mixture which yields a pre-combustion event and pressure rise, followed by a subsequent cool-down. Pressure is monitored during the cool-down and at the desired pressure (temperature) condition, fuel injection is triggered and combustion of the diesel liquid fuel ensues. Full details on this combustion vessel and its use are provided in [8-10].

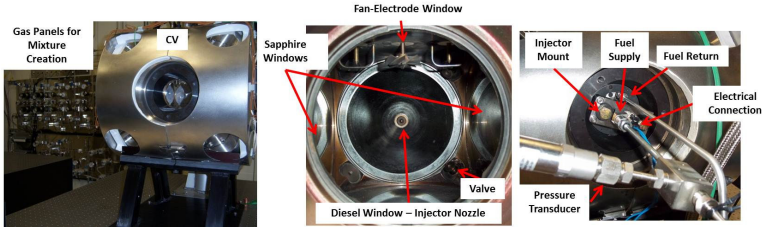

Figure 1: Optically accessible combustion vessel with gas panels for mixture creation (left). Internal view of combustion chamber (center) and external view of diesel injector window (right).

Images are acquired using a Mie back scattering setup, which enables visualization of the liquid phase diesel spray. The setup includes the high speed camera, a Photron Ultima APX RS, equipped with a 50 mm Nikon Nikkor Lens with a f-stop of 1.4. Illumination is provided by a Cooke SensiFlash flashlamp, reflected off a mirror to provide uniform illumination in the CV. Images are acquired with a 2 μs exposure duration, at varying frame rates depending on image resolution. For inert, non-vaporizing images, the resolution is 512x512 at a 10,000 fps frame rate (0.1 ms interframe time). For vaporizing spray tests, images are at 10,000 fps (0.1 ms interframe time) and 512x512 resolution, or at 30,000 fps (0.033 ms interframe time) and 256x256 resolution.

Tests are conducted using ultra-low sulfur diesel fuel. A high pressure (4140 bar) fuel supply system is used to provide the necessary elevated injection pressures. The fuel injector used for this work is the subject of a major development program with demonstrated durability at pressures significantly greater than 3000 bar. The injector used is a 7-hole injector with hole diameters of 0.161 mm and an enclosed angle of 143 degrees. The nozzle needle is low mass and designed to provide fast opening and closing to guarantee maximum spray momentum even with short injection periods. The solenoid injector is driven by a high voltage power supply and switching driver at 42 V, producing an initial peak followed by reduced hold current for the remaining injection duration (electronic trigger), in order to achieve the fastest actuator response whilst maintaining low electrical energy consumption. Control of the fast moving needle is achieved with the next generation, near zero leakage, and fastest response version of Delphi's established 3-way valve solenoid actuator. The accurate control is achieved by ensuring that the flows, unbalanced forces and hence associated valves are as small as possible. Additional details behind this principle are discussed in [11].

Tests include two levels of injection pressure, charge temperature, and charge density. Injection drive duration (electronic trigger length) is set to provide a 1.7ms injection period. Charge-gas density is the density inside the combustion vessel during the experimental test, used to replicate in-cylinder combustion conditions. This includes part-load cases of lower density (7.4 and 14.7 kg/m^3) to represent an engine operating at part-load, and a full load, high density engine operating case of 34.8 kg/m^3.

Image Processing

Images are processed to quantify spray parameters as a function of time after start of injection (ASOI, fuel) for each of the spray plumes. For the inert (non-vaporizing) tests the spray penetration is defined as shown in Figure 2, and for the vaporizing sprays tests the desired parameter is liquid length (LL), defined as the fully connected region from the injector tip. As will be observed in some images, there is a detached fuel slug at the leading edge of the spray. This detaching slug is a discontinuous region of liquid, and therefore is not considered in defining the liquid length. Images are read into MATLAB where the post-processing is performed. The images are then subtracted from the background image (Frame 1), and the background subtracted images are rotated in 51.4 degree increments due to a 7-hole injector to align each spray plume exiting the injector horizontally from left to right. A mask is applied to remove adjacent spray plumes and isolate the spray for processing. The spray image is then converted to black and white using a threshold determined based on the image intensity distribution. A boundary is then traced around the thresholded spray (yellow line in figure below), with the leading edge of the boundary being defined as the penetration of the spray or liquid length for the nonvaporizing and vaporizing sprays respectively (magenta circle in image below). This processing is done for each plume of the image frame, and for each frame of the spray movie to determine the temporal variation of spray properties. Results are presented for the median (from the seven plumes) liquid length or penetration, which provides a repre-

sentative value of the spray characteristics. The median quasi-steady state liquid length is also defined, which is the mean liquid length over the median liquid length temporal data, from 0.3 to 1.2 ms ASOI.

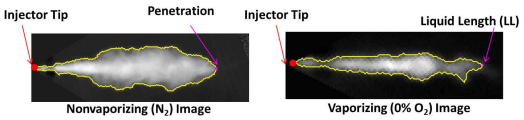

Figure 2: Image processing definitions. Non-vaporizing left and vaporizing right. Yellow line defines traced spray boundary, red circle defines injector tip, magenta circle defines penetration or liquid length.

Spray Penetration Correlation

Experimentally determined penetration results are compared to the spray penetration correlation of Naber and Siebers [7], presented as Equation (1). This correlation predicts full spray penetration as a function of time ASOI, and will be used to compare to non-vaporizing (T=373K) penetration results. Correlation parameters include injection pressure, P_f, charge gas pressure, P_a, charge-gas density, ρ_a, orifice diameter, d_o, and time after start of injection, t.

$$S = A \cdot \sqrt{\sqrt{\frac{P_f - P_a}{\rho_a}} \cdot d_o \cdot t} \qquad (1)$$

The constant, A, is based on representative values for testing including orifice coefficients (velocity and area contraction), cone angle, and another constant [7]. As these injector coefficients were unknown the penetration data versus the square-root of time can be linearly curve fit to define a slope which is the initial term of the equation, providing a value for A once the other constant terms are considered. Applying this correlation to the experimental data showed reasonable agreement; however, it was clear that the square-root time correlation dependence was not matching the overall shape of the experimental data under some conditions.

Therefore, the same general format was used, but a modified curve fit was applied which enabled determination of the optimum curve-fit for the experimental data, with the functional form defined in Equation (2),

$$S = b*(t-a)^m, \qquad (2)$$

where a defines the time shift of the data, m is the exponent of the fit (0.5 in the Naber and Siebers [7] correlation), and b is the curve fit coefficient, which is related to test conditions (fuel and ambient pressure, ambient charge-gas density, and injector orifice diameter as similar to Equation (1), and can be related to the correlation coefficient 'A' value for a direct comparison). Using a non-linear, least squares curve fit methodology, curve fit parameters were determined for the experimental testing. As observed from rate of injection results (not shown) there is a delay between start of current and injector opening of approximately 0.15 ms, as expected, along with a delay to reach a uniform, top-hat rate of injection profile of approximately 0.30 ms relative to start of current. This correlation defines penetration at longer times ASOI when penetration has a non-linear time dependence, before this penetration is linear with time. In the results that follow, only the data from 0.2 ms ASOI and greater was used in the curve fit, to account for the time to reach a relatively steady state rate of injection where the penetration would be expected to follow a power-law trend. Results are shown for the raw data and the experimental curve fits, based on the determined m-exponents. A representative time shift is used from the 34.8 kg/m^3 charge-gas density case. This charge-gas density case is chosen as it has the largest number of data points and therefore results in the best curve fit. Correlation curve fits are displayed based on the time data used in the fits.

Although data is not presented in the paper, one observation to note is that for injection into a 14.7 kg/m^3 charge gas density at 550 bar injection pressure, over 6 repeat tests, the average 'm' exponent was 0.55 and 'A' coefficient was 2.87, showing good agreement to theoretical correlation values of 0.5 and 2.9, respectively as suggested by [7]. As will be shown, values at higher injection pressures show deviation. This leads to the conclusion that reduced injection pressures follows expected penetration versus time trends, but, deviation between experimental and originally accepted correlations is amplified at elevated injection pressures, signifying that there is some underlying difference in injector and/or spray characteristics at these injection pressures.

Liquid Length Correlation

Experimentally determined mean quasi-steady-state liquid length results are compared to the Siebers [12] mixing limited liquid length scaling law. This correlation is evaluated using n-heptadecane as a representative diesel fuel with thermo-physical properties determined using the Peng-Robinson equation of state (Refer to [9] for details). The liquid length correlation is defined as:

$$LL = \frac{b}{a} \cdot \sqrt{\frac{\rho_f}{\rho_a}} \cdot \frac{\sqrt{C_a} d_o}{\tan(\theta/2)} \cdot \sqrt{\left(\frac{2}{B}+1\right)^2 - 1}, \qquad (3)$$

where a and b are constants with values 0.66 and 0.41, respectively, ρ_f is the density of n-heptadecane evaluated at the fuel injection temperature (418 K or 145°C), and C_a is the area-contraction coefficient of the injector, assumed to be 0.8. θ is the cone angle of the spray calculated from Siebers [6],

$$\tan(\theta/2) = 0.26\left[\left(\frac{\rho_a}{\rho_f}\right)^{0.19} - 0.0043 * \sqrt{\frac{\rho_f}{\rho_a}}\right]. \quad \textbf{(4)}$$

The term B in equation (3) is the evaporation coefficient. This is the ratio of fuel and ambient gas mass flow rates which results in complete fuel vaporization, and is defined as:

$$B = \frac{Z_a(T_s, P_a - P_s)\cdot P_s \cdot M_f}{Z_f(T_s, P_s)\cdot [P_a - P_s]\cdot M_a} = \frac{h_a(T_a, P_a) - h_a(T_s, P_a - P_s)}{h_f(T_s) - h_f(T_f, P_a)}, \quad \textbf{(5)}$$

h are component enthalpies, Z is compressibility, P is pressure, T is temperature and M is molecular weight, for ambient a, fuel f, or saturation conditions s, subscripts. The correlation uses ambient conditions of the core of the vessel, which differ from bulk gas conditions presented here due to boundary layers. Core charge-gas conditions are calculated from experimentally measured bulk charge-gas conditions using methods discussed in [7,9].

Results and Discussion

Results are separated into two sections, non-vaporizing and then vaporizing. Results include sample images and spray characteristics determined from images at the different conditions. Penetration and liquid length results are compared to correlations to understand if trends follow previous studies at lower pressures.

Non-vaporizing Diesel Sprays

Density Sweep – 1950 Bar injection Pressure

The influence of charge density on liquid penetration at 1950±10 bar injection pressure into nitrogen was investigated. Images and processed results for the median penetration compared to the power-law correlation fit are shown in Figure 3. As density is increased, penetration is reduced. The exponent from equation (2) of the fit ranges from 0.39 at 7.5 and 14.9 kg/m^3 charge-gas density, to 0.56 at 34.8 kg/m^3 charge gas density. For these test conditions, the highest density case shows the best agreement with the accepted correlation 'm' exponent, when compared to the lower density cases. For the other test conditions, deviations could be attributed to the amount of experimental data points, limited based on camera frame rates or could be due to the constant term in the correlation. Agreement improves at longer times ASOI. Non-zero penetration is shown at negative times ASOI since it takes time for the injector to reach a full rate of injection profile for a fully developed spray.

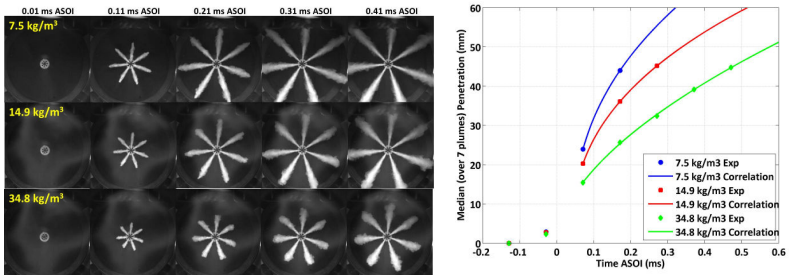

Figure 3: Density sweep images (left) and penetration (right) at 1950 bar injection pressure for non-vaporizing spray tests.

Density Sweep – 2500 Bar injection Pressure

Injection pressure is increased to 2500 ± 10 bar to again examine the impact of charge-gas density on penetration, with images and median penetration results shown in Figure 4. As charge-gas density is increased, experimental median penetration is reduced. The shape of the experimental data differs from the predicted square-root time dependence, with the time exponent ranging from 0.37 to 0.40. Therefore, at elevated injection pressures, there are differences in the time based penetration trends.

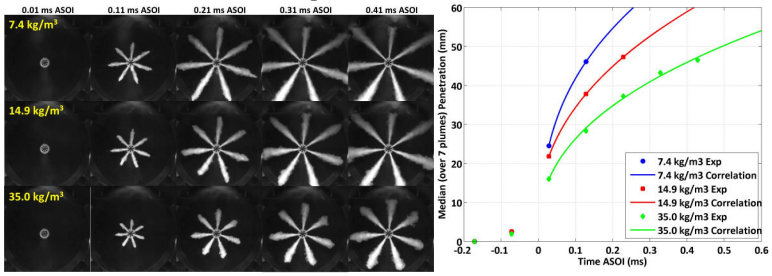

Figure 4: Density sweep images (left) and penetration (right) at 2500 bar injection pressure for non-vaporizing spray tests.

Density Sweep – 2990 Bar injection Pressure

The injection pressure is further increased to its highest value examined of 2990±10 bar to again determine the impact of charge-gas density on penetration, with images and results shown in Figure 5. As charge-gas density is increased, experimental median penetration is reduced as expected both in the images and from the correlation. The experimental data at low charge-gas density has minimal data points in the correlation curve fit and therefore is not an optimal fit. For the 14.8 and 34.9 kg/m^3 charge-gas densities, there are large variations between time-exponents, being 0.37 and 0.49 for the 14.8 and 34.9 kg/m^3 charge gas density cases, respectively.

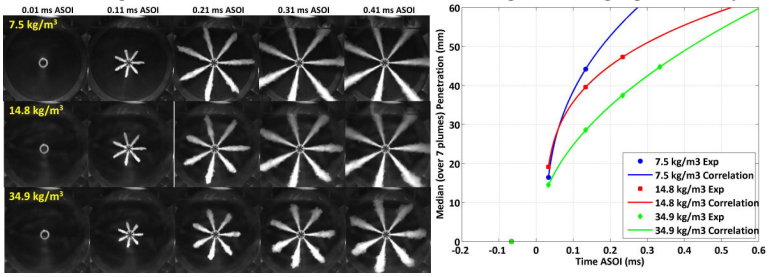

Figure 5: Density sweep images (left) and penetration (right) at 2990 bar injection pressure for nonvaporizing spray tests.

Injection Pressure Sweep – 34.9 kg/m^3 Charge-Gas Density

The effect of increasing injection pressure from 1940 to 3000 bar at the highest charge gas density of 34.9 ± 0.1 kg/m^3 is shown in Figure 6. In this figure are images and results for median penetration as a function of time ASOI for the experimental results and correlation prediction. As injection pressure is increased, penetration is increased, the difference being most pronounced with an injection pressure increase from 1940 to 2500 bar, as opposed to an increase from 2500 to 3000 bar. The correlation time-based exponent ranges from 0.56, to 0.40 and 0.49 for injection pressure increasing from 1940 to 3000 bar. Results (not shown) in regards to trends are similar at the 7.5 and 14.9 kg/m^3 charge-gas density condition.

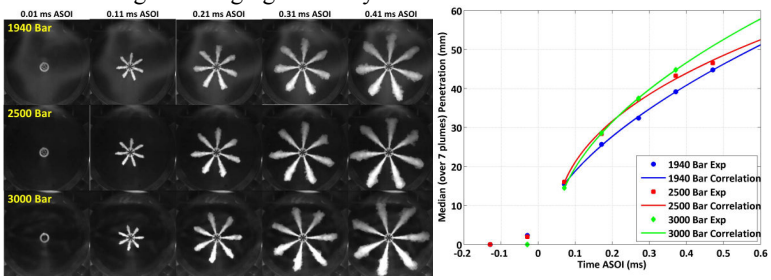

Figure 6: Injection pressure sweep images (left) and penetration (right) at34.9 kg/m^3 charge-gas density for non-vaporizing spray tests.

Vaporizing Diesel Sprays

Vaporizing diesel spray results are presented, which consist of injecting diesel fuel into a high temperature, zero percent oxygen environment created using a preburn procedure. Using the Mie back scattering diagnostic, the liquid phase of the spray is visualized. This liquid penetration reaches a quasi-steady value known as the liquid length, which fluctuates plume to plume and also with time ASOI [10].

Density Sweep – 1105 K Bulk Charge Gas Temperature, 2000 Bar injection Pressure

Tests are conducted at both a part load density (14.6 kg/m^3) and full load density condition (34.6 kg/m^3). Images and liquid length results are shown in Figure 7.

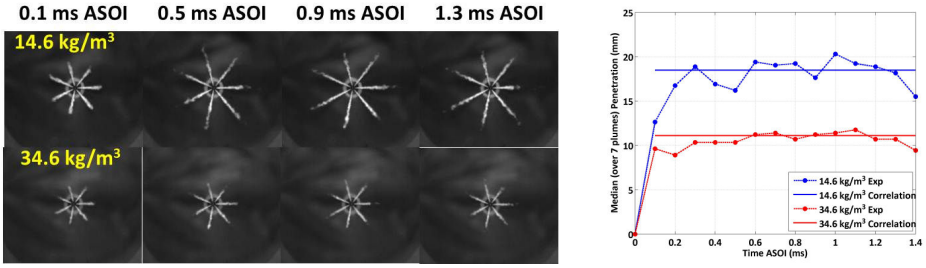

Figure 7: Influence of charge-gas density on vaporizing spray images (left) and median liquid length (right) compared to correlation (solid lines) at 1105 K bulk temperature and 2000 bar injection pressure.

As observed in the images as charge-gas density increases, liquid length reduces by 39%, also agreeing with literature [6]. The median quasi-steady state liquid length, is 19.5 mm at 14.6 kg/m^3 density. This reduces to 11.8 mm at 34.6 kg/m^3 charge-gas density. Correlation results predict a liquid length of 18.5 mm at 14.6 kg/m^3 density or a difference of 5%, and predict a liquid length of 11.1 mm at 34.6 kg/m^3 charge gas density, a difference of 6% relative to experimental. As density increases, liquid length is reduced by 39% experimentally, and 40% by the correlation. At 2000 bar injection pressure and this density range, correlation and experimental results agree within expectation based on correlation assumptions and experimental uncertainty.

Density Sweep – 1100 K Bulk Charge Gas Temperature, 3025 Bar injection Pressure

Tests were conducted at both a part load density (14.6 kg/m^3) and full load density condition (34.7 kg/m^3), with images and liquid length results shown in Figure 8. Note that the images at the full-load density condition were acquired at a higher frame rate of 30,000 fps and hence a reduced resolution, which has caused image scaling as displayed to differ between the two density tests. As charge gas density increases liquid length is reduced as expected. The median quasi-steady state LL is 18.9 mm at 14.6 kg/m^3 charge gas density, and is reduced to 11.8 mm at 34.7 kg/m^3 charge gas density, a decrease of 38%. Correlation results predict a reduction in LL from 18.5 mm to 11.1 mm for this density change, a reduction of 40%. Percent difference between experimental and correlation results at 14.6 kg/m^3 is 29%. The difference at 34.7 kg/m^3 is 19%.

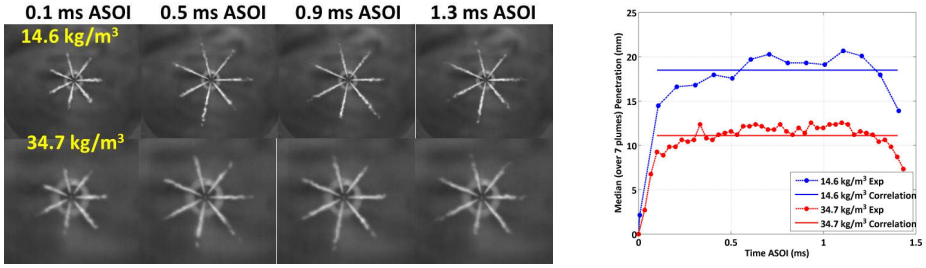

Figure 8: Influence of charge-gas density on vaporizing spray images (left) and median liquid length (right) compared to correlation (solid lines) at 1100 K bulk temperature and 3025 bar injection pressure. Image scaling differs - tests at 34.7 kg/m^3 were acquired at a higher frame rate and reduced resolution.

Injection Pressure Sweep – 1000 K Bulk Charge Gas Temperature, 14.6 kg/m^3 Bulk Charge Gas Density

Injection pressure varied from 1900 to 3020 bar, with images and liquid length results in Figure 9. Images show that as injection pressure increases there are no significant differences in liquid spray behavior in terms of structure in images and penetration. Fluctuations in liquid length are noticed plume to plume, and also frame to frame, showing quasi-steady liquid length behavior [10]. There is only one curve for the correlation as injection pressure does not influence LL and is not a variable in the model [6,12]. As injection pressure increases from 1900 to 3020 bar, there is no noticeable change in liquid length. The steady state liquid length is 21.6 mm at 1900 bar, 21.7 mm at 2440 bar, and 20.5 mm at 3020 bar. The variation is at most 1.2 mm over this 1120 bar injection pressure change. Correlation LL is 21.1 mm, and falls between the experimental liquid lengths.

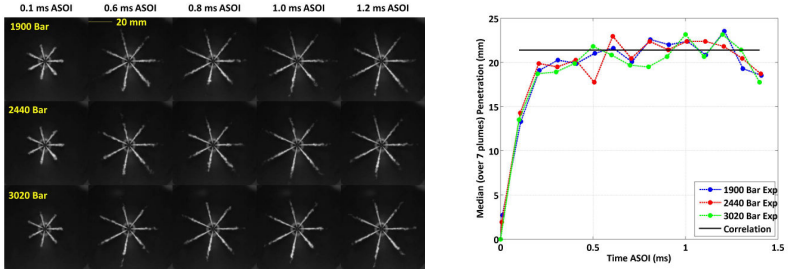

Figure 9: Influence of injection pressure on vaporizing spray images (left) and median liquid length results (right) compared to correlation (solid line) at 1000 K bulk temperature, 14.6 kg/m^3 bulk density.

Injection Pressure Sweep – 1105 K Bulk Charge Gas Temperature, 14.6 kg/m^3 Bulk Charge Gas Density

Injection pressure was changed from 2000 to 3030 bar at 14.6 kg/m^3 bulk charge gas density, and from 2000 to 3020 bar at 34.7 kg/m^3 bulk charge-gas density, liquid length results shown in Figure 10. As injection pressure increases there are no significant differences in liquid length. For the part-load (low density, 14.6 kg/m^3) case, at 2000 bar the quasi-steady liquid length is 19.5 mm, being 18.9 mm at 3030 bar, a difference of 0.6 mm for an injection pressure difference of over 1000 bar. Correlation predicted liquid length is 18.5 mm, at maximum 1 mm difference from the experimental tests. The largest difference between correlation and experimental results is seen at the reduced injection pressure of 2000 bar. For the full-load (34.7 kg/m^3 density case),

the correlation predicted liquid length is 11.1 mm, which is reduced from the experimental quasi-steady state values of 11.8 mm at 2000 bar and 11.8 mm at 3020 bar. There is no difference in liquid length with injection pressure, with experimental results exceeding correlation predicted results by approximately 0.7 mm.

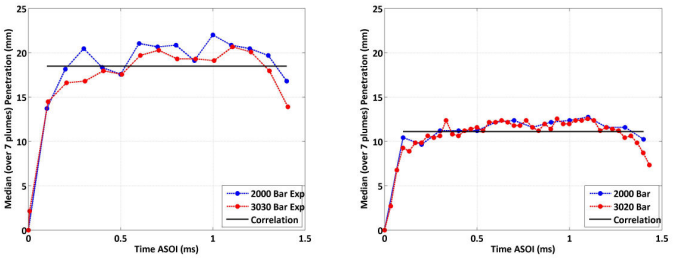

Figure 10: Influence of injection pressure on vaporizing diesel spray median liquid length results compared to correlation (solid line) at 1105 K bulk temperature, 14.6 kg/m^3 bulk charge-gas density (left) and 1100 K bulk charge-gas temperature, 34.7 kg/m^3 bulk charge-gas density (right).

Temperature Sweep – 3030 Bar Injection Pressure, 14.6 kg/m^3 Bulk Charge-Gas Density

Diesel spray vaporization is visualized for charge gas temperatures of 1000 and 1100 K in Figure 11. As charge gas temperature increases, liquid length is visually observed to reduce, as expected based on literature and compared from the experimentally quantified images. The increase in charge gas temperature from 1000 to 1100 K results in a reduction in quasi-steady state LL from 22.0 to 18.9 mm, or 14%. The correlation predicted liquid length, although of reduced magnitude compared to the experimental results, provides a similar percent reduction in LL of 21.1 to 18.5 mm, or 12%.

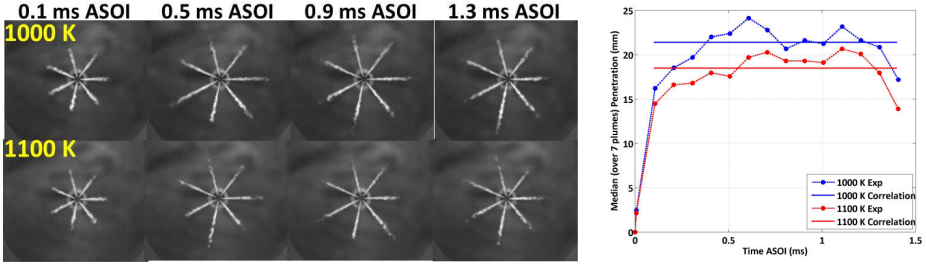

Figure 11: Influence of bulk temperature on vaporizing spray images (left) and median liquid length results (right) compared to correlation (solid line) at 3030 bar injection pressure, 14.6 kg/m^3 bulk density.

Summary and Conclusions

This work investigated the influence of elevated injection pressures on penetration and liquid length spray parameters under non-vaporizing and vaporizing environments, respectively. The quantified spray parameters from image processing are compared to correlation results for both penetration and liquid length. Conclusions are as follows:

Nonvaporizing Sprays

- Increase in injection pressure results in an increase in liquid penetration, being most pronounced at the higher density cases of 14.9 and 34.9 kg/m^3.
- Increase in charge-gas density results in a reduction in liquid penetration.
- The shape of experimental data differs from the predicted square-root time dependence represented by the traditionally accepted correlation of [7], especially at the lowest charge-gas density case. This led to a power-law based curve fitting method, which provides improved agreement between experimental and curve fit results. The time-based exponent values vary, with some showing a near square-root dependence with a 0.5 exponent, and others yielding reduced exponents, down to 0.39. In addition to the exponent differences, the initial coefficient also differs from the expected '*A*' value of 2.9, ranging from 3 up to 12, showing a significant variation in the experimental results power-law fit compared to the correlation.

Vaporizing Sprays

- Increase in injection pressure up to 3000 bar result in no significant change in liquid length. The tests where injection pressure was varied saw at most a 1.2 mm change in liquid length for a 1000 bar change in injection pressure, with the correlation having no dependence of injection pressure on liquid length.

- Increase in charge-gas density results in a reduction in liquid length, by 39% at 2000 bar, and 38% at 3025 bar. The correlation results predict a 40% decrease in liquid length due to this charge-gas density increase. These are within experimental repeatability and measurement uncertainty.
- Increase in charge-gas temperature from 1000 to 1100K results in a 13% and 14% reduction in liquid length at 2000 and 3020 bar, respectively. Correlation results also predict a 13% change in LL for this temperature change.
- Correlation results were consistently less than the experimental results by up to 1 mm, with these differences being attributed to limitations in the correlation and nozzle parameters.

Overall Impact of Elevated Injection Pressures to 3000 Bar

- As injection pressure increases, the trends for experimental liquid length and penetration remain as expected based on reduced injection pressure studies. There is no influence of injection pressure on liquid length under vaporizing conditions, and there is an increase in penetration with an increase in injection pressure, under non-vaporizing conditions.
- The elevated injection pressure conditions for non-vaporizing sprays are best fit with a power-law curve fit, as opposed to using the standard accepted correlation [7].
- For vaporizing sprays, although the correlation typically under-predicts the liquid length, there are no pronounced differences as injection pressure increases. This liquid length correlation is therefore able to predict liquid length parameters at elevated injection pressures, without deviations, under the charge-gas and temperature conditions studied in this work.

Future work will involve the study of this injector under combusting conditions using natural luminosity imaging, laser induced incandescence (LII) for relative soot measurements, and chemiluminescence for defining lift-off length to further understand the influence of these elevated injection pressures on fundamental spray and combustion characteristics.

Acknowledgements

Acknowledgements are provided to AVL and Delphi Diesel Systems for their support of this work. Further acknowledgement is given to the National Science Foundation for the funding of MRI grant number 0619585 for the development of this optically accessible combustion vessel laboratory. Acknowledgement is also given to A&D Technology for their assistance in providing the data acquisition system.

References

1. Jones, T.O., "Assessment of Technologies for Improving Light Duty Vehicle Fuel Economy: Letter Report, 2010," *The National Academies,* Available from: http://www.nap.edu/catalog/12163.html, 2008.
2. Mahr, B., "Future and Potential of Diesel Injection Systems," *THIESEL 2002 Conference on Thermo- and Fluid-Dynamic Processes in Diesel Engines,'* 2002.
3. National Academies Press (NAP), 'Technologies and Approaches to Reducing the Fuel Consumption of Medium- and Heavy-Duty Vehicles,' *Committee to Assess Fuel Economy Technologies for Medium- and Heavy-Duty Vehicles,* Washington, DC, http://books.nap.edu/catalog.php?record_id=12845, 2010.
4. Wloka, J.A., Pflaum, S., Wachtmeister, G., *SAE 2012-01-1131*, 2010.
5. Siebers, D.L., *SAE 852102,* 1985.
6. Siebers, D.L., *SAE 980809*, 1998.
7. Naber, J.D., Siebers, D.L., *SAE 960034*, 1996.
8. Johnson, J.E., Naber, J.D., Lee, S-.Y., Kurtz, E., Robarge, N., Ge, H.-W., *SAE 2012-01-0455*, 2012.
9. Nesbitt, J.E., "Diesel Spray Mixing Limited Vaporization with Non-Ideal and Multi-Component Fuel Thermophysical Property Effects," Thesis for the Degree of Doctor of Philosophy in Mechanical Engineering, Michigan Technological University, 2011.
10. Nesbitt, J.E., Naber, J.D., Lee, S-.Y., Kurtz, E., Ge, H-.W., Robarge, N., ILASS Americas 23rd Annual Conference on Liquid Atomization and Spray Systems, 2011, Paper No. 132.
11. Hardy, C.S., Hudson, C.M., Harper, M.S., Ainsworth, D.M., "Pressure is nothing without control: Evolution of Control Valve Design," IMechE Conference on Fuel Systems for IC Engines, March 2012.
12. Siebers, D.L., *SAE 1999-01-0528,* 1999.